PERGAMON

International Journal of Heat and Mass Transfer 45 (2002) 1595–1603

International Journal of HEAT and MASS TRANSFER

www.elsevier.com/locate/ijhmt

Numerical study of thermal instability in mixed convection flow over horizontal and inclined surfaces

Ming-Han Lin [a,*], Chin-Tai Chen [b]

[a] Department of Automation Engineering, Ta-Hwa Institute of Technology, Hsinchu 307, Taiwan, ROC
[b] Department of Industrial Engineering and Management, Ta-Hwa Institute of Technology, Hsinchu 307, Taiwan, ROC

Received 20 October 2000; received in revised form 7 September 2001

Abstract

This paper presents numerical study of thermal instability in mixed convection flow over horizontal and inclined plates. The criterion on the position marking on the onset of longitudinal vortices is defined in the present paper. The results show that the onset position characterized by the Grashof number depends on the Prandtl number, wave number, and the inclined angle ϕ from the horizontal. The flow is found to become more stable to the vortex mode of instability as the value of inclined angle increases, owing to a decrease in buoyancy force in the normal direction. However, the Prandtl number has a destabilizing effect on the flow. The results of the present numerical prediction show reasonable agreement with the experimental data in the literature.

Keywords: Mixed convection; Grashof number; Longitudinal vortices; Thermal instability

1. Introduction

The problem of the thermal instability in a laminar mixed convection flow over horizontal and inclined plates has received attention in the heat transfer literature. The understanding of thermal and flow characteristics in buoyancy force driven vortex flow is important in the design of compact heat exchanger [1], cooling of microelectric equipment [2], and chemical vapor process [3]. It is advantageous to suppress the vortices so as to achieve uniform deposition in chemical vapor deposition processes. In contrast, it is desirable to enhance the vortices so as to induce earlier transition to turbulence and increase heat transfer from the surface in surface cooling.

There is a large body of literature on the thermal instability in mixed convection flow over horizontal and inclined plates (e.g., [4–6], etc.). However, quantitative agreement between theory and experiment for the onset of vortex instability of the flow under consideration is still unsatisfactory. The discrepancy between the theoretical critical values of Grashof number and those experimental data were one to two orders in the literature. By reviewing the criteria of the onset of the longitudinal vortices in boundary layer and channel flows, the experimental and numerical methods employed in the literature for determining the onset of longitudinal vortices were summarized in [7].

The attempt of this paper is to present numerical experiment for the onset and subsequent linear development of longitudinal vortices in mixed convection flow over horizontal and inclined plates. The experimental criteria proposed by Hwang and Lin [7] for the onset of longitudinal vortices were employed in the present study. The governing parameters on the onset of longitudinal vortices are the Prandtl number, the wave number a, the inclined angle ϕ from the horizontal, and the Grashof number. In the computation, the Prandtl number is 0.7 (for air) and 7.0 (for water), the inclined angle from the horizontal $\phi = 0°$, 5°, 10°, 15°, 20°, 30°, 45°, 60°, and 70°, the magnitudes of imposed initial disturbance temperature $t^0 = 10^{-4}$, and the flat plate length parameter $Gr_L/Re_L^{3/2} = 500$.

* Corresponding author. Tel.: +886-3-5927700x2660; fax: +886-03-5921047.
E-mail address: aemhlin@et4.thit.edu.tw (M.-H. Lin).

0017-9310/02/$ - see front matter
PII: S0017-9310(01)00283-6

Nomenclature

a'	dimensional wave number, $a' = 2\pi/\lambda$ (1/m)
a	dimensionless wave number, $a = a'L/Re_L^{1/2}$
F	velocity, pressure or temperature function
f	reduced stream function, $\psi/(vXU_\infty)^{1/2}$
Gr_X	local Grashof number, $Gr_X = (g\beta(T_w - T_\infty)X^3)/v^2$
h	local heat transfer coefficient ($W/(m^2/K^{-1})$)
Nu_X	local Nusselt number, hX/k
p', p	dimensional and dimensionless pressure, $p' = \rho U_\infty^2 p/Re_L$
Pr	Prandtl number, v/α
Re_X	local Reynolds number, $Re_X = U_\infty X/v$
T	temperature (K)
t', t	dimensional and dimensionless perturbation temperature, $t' = (T_w - T_\infty)t$ (K)
t^0	initial constant perturbation temperature at $x = 0$ (K)
U, V, W	dimensional velocity components (m/s)
u, v, w	dimensionless perturbation velocity components
u', v', w'	perturbation velocity components (m/s)
X, Y, Z	Cartesian coordinates (m)
x, y, z	dimensionless Cartesian coordinates as defined in (14)

Greek letters

α	thermal diffusivity of fluid (m^2/s)
β	coefficient of thermal expansion (1/K)
δ	boundary layer thickness (m)
η	similarity variable, $Y(U_\infty/vX)^{1/2} = y/\sqrt{x}$
θ_b	dimensionless basic temperature, $(T - T_\infty)/(T_w - T_\infty)$
λ	wavelength in Z-direction (m)
v	kinematic viscosity of fluid (m^2/s)
ξ	vorticity function in X-direction defined in (15)
ψ	stream function (m^2/s)

Superscripts

$-$	dimensionless quantities
$*$	onset position
$'$	disturbance quantity or derivative with respect to η

Subscripts

b	basic flow quantity
L	quantity based on the plate length
p	perturbation quantity
w	wall condition
X	local coordinate
∞	free stream condition

2. Theoretical analysis

Consider a laminar mixed convection flow over horizontal and inclined heated plates with a free stream velocity U_∞, as shown in Fig. 1. The acute angle of inclination from the horizontal is ϕ. The physical Cartesian coordinates are chosen such that X measures the streamwise distance from the leading edge of the plate, Y is the distance normal to the plate, and Z is in the transverse direction. The streamwise and normal velocity components are U_b and V_b. The governing boundary layer equations for constant-property fluids under the Boussinesq approximation can be written as

$$\frac{\partial U_b}{\partial X} + \frac{\partial V_b}{\partial Y} = 0, \tag{1}$$

$$U_b\frac{\partial U_b}{\partial X} + V_b\frac{\partial U_b}{\partial Y} = v\frac{\partial^2 U_b}{\partial Y^2} + g\beta\cos\phi\frac{\partial}{\partial X}\int_Y^\infty (T_b - T_\infty)\,dY + g\beta(T_b - T_\infty)\sin\phi, \tag{2}$$

$$U_b\frac{\partial T_b}{\partial X} + V_b\frac{\partial T_b}{\partial Y} = \alpha\frac{\partial^2 T_b}{\partial Y^2}, \tag{3}$$

where T_w is the surface temperature, and T_∞ is the free-stream temperature.

Next, one introduces the following dimensionless variables and parameters:

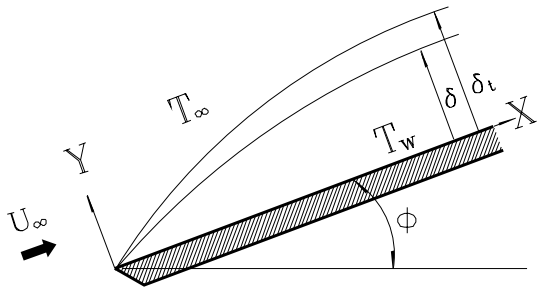

Fig. 1. Physical configuration and coordinate system.

$$
\begin{aligned}
&X = Lx,\\
&Y = LRe_L^{-1/2}y,\\
&U_b = U_\infty \bar{u},\\
&V_b = U_\infty Re_L^{-1/2}\bar{v},\\
&\theta_b = \frac{T_b - T_\infty}{T_w - T_\infty},\\
&\eta = Y(U_\infty/vX)^{1/2},\\
&f(X,\eta) = \psi/(vXU_\infty)^{1/2},
\end{aligned}
\tag{4}
$$

where $f(X,\eta)$ is the reduced stream function. The basic flow equations (1)–(3) transformed from (X,Y) into (x,η) plane are:

$$
\begin{aligned}
&f''' + \left(\frac{1}{2}f + x\frac{\partial f}{\partial x}\right)f'' - xf'\frac{\partial f'}{\partial x}\\
&\quad = -\frac{Gr_L}{Re_L^2}x\theta_b \sin\phi - \frac{Gr_L}{Re_L^{5/2}}\sqrt{x}\\
&\qquad \times \left[\frac{1}{2}\int_\eta^\infty \theta_b \,\mathrm{d}\eta + \frac{1}{2}\eta\theta_b + x\int_\eta^\infty \frac{\partial\theta_b}{\partial x}\,\mathrm{d}\eta\right]\cos\phi,
\end{aligned}
\tag{5}
$$

$$
\theta_b'' + \left(\frac{1}{2}f + x\frac{\partial f}{\partial x}\right)Pr\,\theta_b' - xPrf'\frac{\partial\theta_b'}{\partial x} = 0. \tag{6}
$$

The boundary conditions are as follows:

$$
\begin{aligned}
&f(x,0) = f'(x,0) = \theta_b(x,0) - 1 = 0,\\
&f'(x,\infty) - 1 = \theta_b(x,\infty) = 0.
\end{aligned}
\tag{7}
$$

In Eqs. (5)–(7), the primes denote partial derivatives with respect to η and Pr is the Prandtl number.

2.1. Perturbation equations

In the region near or upstream of the onset position x^*, the disturbances of longitudinal vortex type are small and the nonlinear terms in the momentum and energy equations may be linearized. Furthermore, in experiments ([5,8–10], etc.), 'stationary' longitudinal vortex rolls have been found periodic with a wavelength λ in the transverse direction Z. Therefore, the disturbances superimposed on the two-dimensional basic flow quantities can be expressed as

$$
\begin{aligned}
&F(X,Y,Z) = F_b(X,Y) + \zeta(X,Y)\,\exp(\mathrm{i}a'Z),\\
&W(X,Y,Z) = w'(X,Y)\,\mathrm{i}\,\exp(\mathrm{i}a'Z),
\end{aligned}
\tag{8}
$$

where $F = U,V,P$ or T, $\zeta = u',v',p'$ or t'. The value $a' = 2\pi/\lambda$ is the dimensional transverse wave number of the vortex rolls. By consideration of the vortex-type perturbation quantities in continuity equation, a different expression for W is used.

Substituting Eq. (8) into the continuity, Navier–Stokes, and energy equations in Cartesian coordinates, and subtracting the two-dimensional basic flow and energy equations under the assumptions of $Gr_L \gg 1$ and $Re_L \gg 1$, one can obtain the linearized perturbation equations:

$$
\frac{\partial u'}{\partial X} + \frac{\partial v'}{\partial Y} - a'w' = 0, \tag{9}
$$

$$
\begin{aligned}
&U_b\frac{\partial u'}{\partial X} + u'\frac{\partial U_b}{\partial X} + V_b\frac{\partial u'}{\partial Y} + v'\frac{\partial U_b}{\partial Y}\\
&\quad = g\beta t'\sin\phi + v\nabla^2 u',
\end{aligned}
\tag{10}
$$

$$
\begin{aligned}
&U_b\frac{\partial v'}{\partial X} + u'\frac{\partial V_b}{\partial X} + V_b\frac{\partial v'}{\partial Y} + v'\frac{\partial V_b}{\partial Y}\\
&\quad = g\beta t'\cos\phi - \frac{1}{\rho}\frac{\partial p'}{\partial Y} + v\nabla^2 v',
\end{aligned}
\tag{11}
$$

$$
U_b\frac{\partial w'}{\partial X} + V_b\frac{\partial w'}{\partial Y} = -\frac{1}{\rho}a'p' + v\nabla^2 w', \tag{12}
$$

$$
U_b\frac{\partial t'}{\partial X} + V_b\frac{\partial t'}{\partial Y} + u'\frac{\partial T_b}{\partial X} + v'\frac{\partial T_b}{\partial Y} = \alpha\nabla^2 t', \tag{13}
$$

where β is coefficient of thermal expansion, and $\nabla^2 = (\partial^2/\partial Y^2) - a'^2$ is a two-dimensional Laplacian operator. The perturbation equations are two-dimensional and of boundary layer flow type.

Next, on the top of Eq. (4), one introduces the following dimensionless variables and parameters:

$$
\begin{aligned}
&Z = LRe_L^{-1/2}z,\\
&u' = U_\infty u,\\
&[v'\ \ w'] = U_\infty Re_L^{-1/2}[v\ \ w],\\
&t' = (T_w - T_\infty)t,\\
&p' = \frac{\rho U_\infty^2}{Re_L}p,\\
&a' = \frac{Re_L^{1/2}}{L}a,\\
&Re_L = \frac{U_\infty L}{v},\\
&Gr_L = \frac{g\beta(T_w - T_\infty)L^3}{v^2},
\end{aligned}
\tag{14}
$$

and a vorticity function in the axial direction

$$
\xi = \frac{\partial w}{\partial y} - av. \tag{15}
$$

To obtain equation for the vorticity, one may differentiate Eqs. (11) and (12) by z and y, respectively, and then eliminate the pressure terms by subtracting one from another. To derive the equation for v, one may differentiate Eq. (15) with respect to z. Similarly, the equation for w can be obtained by differentiating Eq. (15) by y. It is noted that in the derivation of equations for v and w, Eq. (15) or continuity equation (9) must be considered. By using also the similarity variable $\eta = y/\sqrt{x}$, the perturbation equations in η and x planes are found:

$$\frac{\partial^2 u}{\partial \eta^2}+\left(\frac{1}{2}f+x\frac{\partial f}{\partial x}\right)\frac{\partial u}{\partial \eta}-xf'\frac{\partial u}{\partial x}-\left(a^2x+x\frac{\partial f'}{\partial x}-\frac{1}{2}\eta f''\right)u=f''\sqrt{x}v-\frac{Gr_L}{Re_L^2}xt\sin\phi, \tag{16}$$

$$\frac{\partial^2 t}{\partial \eta^2}+\left(\frac{1}{2}f+x\frac{\partial f}{\partial x}\right)Pr\frac{\partial t}{\partial \eta}-xf'Pr\frac{\partial t}{\partial x}-a^2xt=Pr\frac{\partial \theta_b}{\partial \eta}\left(-\frac{1}{2}\eta u+\sqrt{x}v\right)+Pr\,ux\frac{\partial \theta_b}{\partial x}, \tag{17}$$

$$\frac{\partial^2 \xi}{\partial \eta^2}+\left(\frac{1}{2}f+x\frac{\partial f}{\partial x}\right)\frac{\partial \xi}{\partial \eta}-xf'\frac{\partial \xi}{\partial x}-\left(\frac{1}{2}\eta f''+a^2x-x\frac{\partial f'}{\partial x}\right)\xi=x\frac{Gr_L}{Re_L^{3/2}}at\cos\phi-au\left(\frac{1}{4\sqrt{x}}(f-\eta f'-\eta^2 f'')+\sqrt{x}\left(\eta\frac{\partial f'}{\partial x}-\frac{\partial f}{\partial x}\right)-x^{3/2}\frac{\partial^2 f}{\partial x^2}\right)+\sqrt{x}f''\left(\frac{\partial w}{\partial x}-\frac{\eta}{2x}\frac{\partial w}{\partial \eta}\right), \tag{18}$$

$$\frac{\partial^2 v}{\partial \eta^2}-xa^2v=ax\xi-\sqrt{x}\frac{\partial^2 u}{\partial x\partial \eta}+\frac{1}{2\sqrt{x}}\eta\frac{\partial^2 u}{\partial \eta^2}+\frac{1}{2\sqrt{x}}\frac{\partial u}{\partial \eta}, \tag{19}$$

$$\frac{\partial^2 w}{\partial \eta^2}-xa^2w=\sqrt{x}\frac{\partial \xi}{\partial \eta}-ax\frac{\partial u}{\partial x}+\frac{1}{2}a\eta\frac{\partial u}{\partial \eta}. \tag{20}$$

The set of equations (16)–(20) is a boundary value problem in η-direction, an initial value problem in x-direction, and an eigenvalue problem in z-direction. The appropriate initial condition and boundary conditions of the perturbations equations are

$$\begin{aligned} &u=v=w=t=0 \quad \text{at } \eta=0,\\ &u=v=w=t=\xi=0 \quad \text{at } \eta=\infty,\\ &u=v=w=\xi=t-t^0=0 \quad \text{at } x=0. \end{aligned} \tag{21}$$

An initial value (Eq. (21)) is set at $x=0$. However, the perturbation equations (16)–(20) are computed at $x>0$. Thus, the singularity point $x=0$ is removed. For simplicity, the initial amplitude function t^0 is set uniform, and the other velocity components u, v, and w are set zero. However, the magnitudes of the velocities u, v, and w will be generated in the next x-steps. The magnitude of the initial amplitude function, $t^0=10^{-4}$ is used in the present study.

Eqs. (16)–(20) and boundary conditions (21) in the x–η plane are for unknowns u, t, ξ, v, and w with three fixed values of a, Re_L, and Gr_L. By giving a series value of a, the largest amplification of the perturbation quantities along the x-direction determines the value of critical wave number a^*. One may prove analytically the homogeneity of L for $\phi=0°$ in Eqs. (16)–(20) by considering the dimensionless transformations (14), i.e., $v\sim L^{1/2}$, $w\sim L^{1/2}$, $a\sim L^{1/2}$, $x\sim L^{-1}$, $y\sim L^{-1/2}$, $z\sim L^{-1/2}$, and $\xi\sim L$ (variables of η and f are independent of L). In the computation, the selection of Re_L and Gr_L does not change the local critical Grashof number $(Gr_X/Re_X^{3/2})^*$ and the critical wave number $(ax^{1/2})^*$. This is also proved by using several values of Re_L and Gr_L in computation. The present study, $Gr_L/Re_L^{3/2}=500$ is used for demonstrating the results.

The local Nusselt number of the basic and perturbed flows can also be expressed as

$$\begin{aligned} Nu_X&=Nu_b+Nu_p\\ &=\frac{(h_b+h_p)X}{k}\\ &=-Re_X^{1/2}\left[\theta_b'(x,0)+\left.\frac{\partial t(x,0)}{\partial \eta}\right|_w\right] \end{aligned} \tag{22}$$

or

$$\frac{Nu_X}{Nu_b}=\left[1+\left.\frac{\partial t(x,0)}{\partial \eta}\right|_W\Big/\theta_b'(x,0)\right],$$

where h is the local heat transfer coefficient, the subscripts b and p indicate the basic and perturbed flows, and k is the fluid thermal conductivity. It is noted that Nu_X is based on the thermal boundary condition of constant wall temperature.

3. Numerical procedure

A finite difference scheme based on the weighting function [11] with second-order accuracy in both η and x is used. The step-by-step procedure is listed as follows:

1. Assign Pr, $Gr_L/Re_L^{3/2}$, Re_L, and ϕ to obtain the basic flow and temperature distributions. The values of Pr are 0.7 (for air) and 7.0 (for water), $Gr_L/Re_L^{3/2}=500$, $Re_L=10^5$, and the values of ϕ are 0°, 5°, 10°, 15°, 20°, 30°, 45°, 60°, and 70°.
2. Assign zero initial values of u, v, w, and ξ, initial temperature at leading edge, $t^0=10^{-4}$ and various values of wave number a.
3. Solve Eqs. (17)–(19) for u, t and ξ distributions at the next x-step. Values of ξ on boundary are evaluated with previous iteration data of v and w in the interior region.
4. Solve Eqs. (20) and (21) for v and w with the obtained u and ξ.
5. Repeat steps (3) and (4), until the perturbation quantities meet the convergence criteria at the streamwise position:

$$\max\left(\frac{\left|F_{i,j}^{(n+1)}\right|-\left|F_{i,j}^{(n)}\right|}{F_{i,j}^{(n+1)}}\right)\leqslant 10^{-5},$$

where $F_{i,j}^{(n)}$ are the perturbation quantities u, v, w, t, and ξ of nodal point (i,j) at the nth number of iteration.

6. Calculate the local Nusselt number of the vortex flow.
7. Repeat steps (3)–(6) at the next mainstream position until a desired mainstream position is reached.
8. The absolute values of perturbation quantities are growing along the mainstream direction. One can find the mainstream position marked with x_{cr}, where the onset criterion $Nu_p/Nu_b = 0.1$ is satisfied. Various onset positions x_{cr} can be determined for different values of wave number a. The minimum x_{cr} denoted by x^* is the most probable onset position and the corresponding wave number is denoted by a^*. The local critical value is $(Gr_X/Re_X^{3/2})^* = (Gr_L/Re_L^{3/2})x^{*3/2}$ and the local wave number is $a^*x^{*1/2}$ for this computation.

The criterion for determination of the onset of longitudinal vortices using the technique of heat transfer measurement in experiments can be explained as follows:

The experimental and numerical methods employed in the literature for determining the onset of longitudinal vortices were reviewed by Hwang and Lin [7]. There are several ways to set the onset criteria: velocity measurement, temperature measurement, heat transfer measurement, and flow visualization, etc. Although the onset criteria are different, there are on the same of order of magnitude in the critical values of parameters, as pointed by Hwang and Lin [7]. Meanwhile, the onset criteria by heat transfer measurement (Nu_p/Nu_b) are usually used in the experiments ([12–14], etc.). It was known that heat transfer rate can be increased by introducing vortex flow. The onset position can be determined by comparison of the heat transfer rate between the measured values of secondary flow and the basic flow data (6–30% of Nu_p/Nu_b by Incropera et al. [12], 15% of Nu_p/Nu_b by Maughen and Incropera [13], 10% of Nu_p/Nu_b by Chou and Han [14], etc.). Also by comparison of the onset criterion between $Nu_p/Nu_b = 0.2$ and $Nu_p/Nu_b = 0.1$ in the numerical experiment, the values of onset position x^* increases less than 4%. It is reasonable to set $Nu_p/Nu_b = 0.1$ for the onset criterion of longitudinal vortices in the numerical solution by heat transfer measurement techniques.

Table 1 shows a typical result of perturbation temperature development along the x-direction. The grids are uniform in both normal and streamwise directions. Grid sizes of $\Delta x = 0.002$ and 0.001, $\Delta\eta = 0.02$ and 0.01 are used to perform the numerical experiment. The result at $x = 0.5$ has a largest difference of 0.44%, but the difference at $x < 0.4$ is less than 0.44%. The grid sizes of $\Delta x = 0.002$, $\Delta\eta = 0.02$, and $\eta_\infty = 10$ are used to perform the numerical experiment. To check the validity of the linear equations (16)–(20), the order of magnitude of nonlinear terms of perturbation equations near the onset position are checked. The calculated data are substituted into the individual terms of the x-momentum equation. The order of the nonlinear terms is two orders of magnitude smaller than the order of linearized inertia terms. Therefore, the linear theory is valid for the estimation of the onset of longitudinal vortices in a laminar mixed convection flow over horizontal and inclined heated plates.

4. Results and discussion

The typical development of the dimensionless perturbation amplitudes u, v, w, and t at $x = 0.3$, 0.35, and 0.4 for $Pr = 0.7$, $Gr_L/Re_L^{3/2} = 500$, $a^* = 1.38$, and $\phi = 0°$ is shown in Fig. 2. The magnitude of v and w are larger than those of u and t because the scaling factor $Re_L^{-1/2}$ is included in these quantities. The shapes of the v and w profiles may be regarded as a vortex pattern.

Fig. 3 depicts the dimensionless perturbation amplitude functions at $x = 0.76$, 0.8, and 0.84 with the value of inclined angle $\phi = 45°$. It is seen that the values of perturbation amplitude functions are decreased with the stabilizing effect of increased inclined angle ϕ. It is also observed in this figure that the profiles of perturbation amplitude functions are shrunk to smaller η region due to the angle effect. It is noted that a reversed velocity profile near free stream region was induced downstream of the linear development region of longitudinal vortices.

It is also interesting to study numerically the variations of local heat transfer rate after onset of longitu-

Table 1
Grid size test for $Gr_L/Re_L^{3/2} = 500$, $a^* = 1.38$, $Pr = 0.7$, and $\phi = 0°$

Δx	$\Delta\eta$	$x = 0.1$	$x = 0.2$	$x = 0.3$	$x = 0.4$	$x = 0.5$
0.002	0.02	0.01375[a]	0.05848	0.4753	7.227	183.3
0.002	0.01	0.01375	0.05847	0.4751	7.221	183.0
0.001	0.02	0.01375	0.05849	0.4756	7.231	183.8

[a] These are the maximum values of perturbation temperature $t/0.01$ at the specified x position.

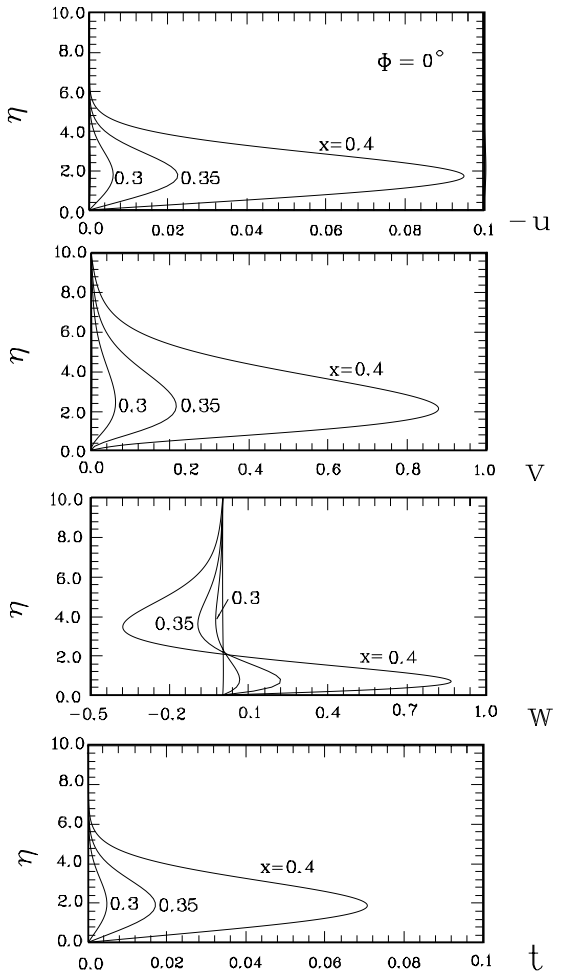

Fig. 2. Development of perturbation amplitude profiles at specified x positions for $Gr_L/Re_L^{3/2} = 500$, $a^* = 1.38$, $\phi = 0°$, and $Pr = 0.7$.

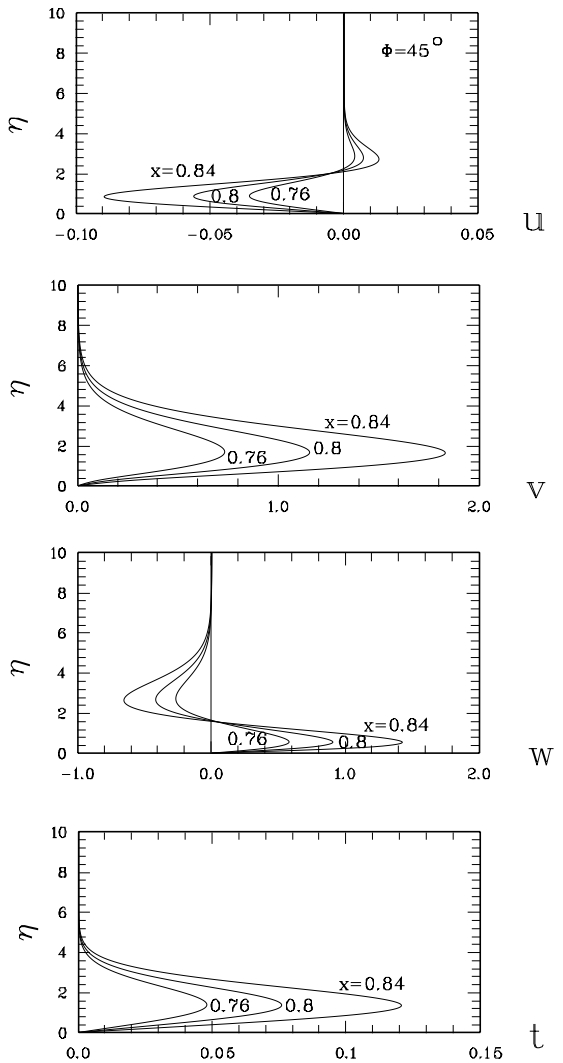

Fig. 3. Development of perturbation amplitude profiles at specified x positions for $Gr_L/Re_L^{3/2} = 500$, $a^* = 1.38$, $\phi = 45°$, and $Pr = 0.7$.

dinal vortices. The perturbation heat transfer rate Nu_p behaves like a cosine function in the Z-direction (i.e., $Nu \propto \partial T/\partial Y \propto \exp(\mathrm{i}a'Z)$). Although the mean values of heat transfer rate in one spanwise wave is zero, the maximum variation of local heat transfer rate along z-direction occurred at $z = 0$ and $z = 2\pi/a$. The variations of local Nu_X/Nu_b along axial direction at $z = 0$ are shown in Fig. 4. The correlation equation for turbulent free convection for horizontal plate is also shown for comparison [15,16], i.e.,

$$Nu_X = 0.13(Pr\,Gr_X)^{1/3}$$

or

$$\frac{Nu_X}{Nu_b} = \frac{0.13(Pr\,Gr_X)^{1/3}}{0.332\,Pr^{1/3}\,Re_X^{1/2}} = 0.39\left(Gr_X/Re_X^{3/2}\right)^{1/3}, \tag{23}$$

where $-\theta_b'(X,0) = 0.332$ at $\phi = 0°$ and $Pr = 0.7$ is chosen for reference.

The gradients of the temperature at the wall start to deviate from the laminar natural convection at downstream of x^*, due to the secondary longitudinal vortex flow on the heated plate. The angle effects on the longitudinal vortices are less pronounced when the values of inclined angle ϕ increases.

The physical meanings of the critical values of $(Gr_X/Re_X^{3/2})^*$, and the local critical wave number $a^*x^{*1/2}$ can be interpreted as follows: they may be converted to $Gr^*_{\delta_r}$ and $a'^*\delta_r$, respectively, by the following transformations:

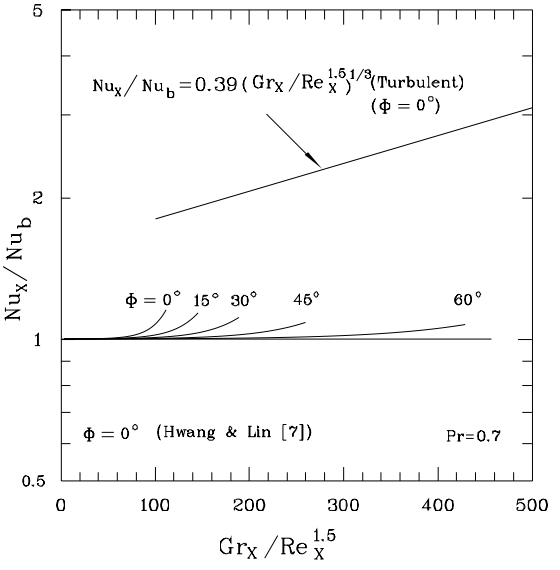

Fig. 4. Local Nusselt number ratio Nu_X/Nu_b vs. $Gr_X/Re_X^{3/2}$ at $z = 0$.

$$Gr^*_{\delta_r} = \frac{g\beta(T_w - T_\infty)}{\nu^2}\left(\frac{X}{Re_X^{1/2}}\right)^{*3} = \left(\frac{Gr_X}{Re_X^{3/2}}\right)^*,$$
$$(a'\delta_r)^* = \left(\frac{2\pi}{\lambda}\frac{X}{Re_X^{1/2}}\right)^* = (ax^{1/2})^*, \tag{24}$$

where the local boundary layer characteristic thickness $\delta_r = X/Re_X^{1/2}$.

The results of the critical Grashof number of Fig. 6 in [7] show good agreement with the previous experimental results for the case of $\phi = 0°$. But the discrepancy of the critical wave number exists among Hwang and Lin [7] and the experimental data. The reason is due to different experimental conditions are set and explained as follows:

By eliminating the boundary layer thickness δ between the parameter Gr_{δ_r} and the wave number $a'\delta_r$ of Eq. (24), we may obtain the relation

$$\frac{Gr^*_{\delta_r}}{(a'\delta_r)^{*3}} = \left(\frac{Gr_L}{Re_L^{3/2}}\right)^* \Big/ a^{*3} = K \quad \text{or} \quad Gr^*_{\delta_r} = K(a'\delta_r)^{*3}. \tag{25}$$

Eq. (25) indicated that the wavelength of the longitudinal vortices are kept constant in the downstream. The growth of the vortices with constant wavelength can be shown by straight lines of gradient 3 on a logarithmic scale. It is noted that the value of K can be determined by the assigned $Gr_L/Re_L^{3/2}$, and the obtained critical wave number a^*. For $Gr_L/Re_L^{3/2} = 500$ and $a^* = 1.38$, $K = 190$ is calculated.

Moreover, by considering Eq. (25) and keeping constant Gr_{δ_r}, then $\delta_r \propto \beta^{-1/3}\Delta T^{-1/3}\nu^{2/3}$, one may modify the data $(a'\delta_r)^*$ in experiments by the following transformations:

$$(a'\delta_r)^*_{mod} = \frac{(a'\delta_r)^*_r}{(a'\delta_r)^*_{exp}}(a'\delta_r)^*_{exp} = \left(\frac{\lambda_{exp}}{\lambda_r}\right)\left(\frac{\beta_{exp}}{\beta_r}\right)^{1/3}\left(\frac{\Delta T_{exp}}{\Delta T_r}\right)^{1/3} \times \left(\frac{\nu_{exp}}{\nu_r}\right)^{-2/3}(a'\delta_r)^*_{exp} \tag{26}$$

or

$$(a'\delta_r)^*_{mod} = \left(\frac{\left(Gr_L/Re_L^{3/2}\right)_{exp}}{\left(Gr_L/Re_L^{3/2}\right)_r}\right)^{1/3}\frac{a_r}{a_{exp}}(a'\delta_r)^*_{exp},$$

where the subscripts mod, r, and exp denote modified, reference and experimental conditions, respectively. For example, $U_r = 1$ m/s, $L_r = 1$ m, $\Delta T_r = 10$ K, $\beta_r = 1/293$ K^{-1}, $\nu_r = 1.56 \times 10^{-5}$ m^2/s (air at 20° and atmospheric pressure), and

$$\lambda_r = \frac{2\pi}{a^*}\sqrt{\frac{\nu_r L_r}{U_r}} = 0.018 \text{ m}$$

are set in the present study. Fig. 5 replots the results of Hwang and Lin [7] and previous experimental data for the onset of longitudinal vortices in a mixed convection flow over horizontal and inclined plate for $Pr = 0.7$. The experimental data, including two air data, and covering the range $U_{exp} = 0.1$–0.6 m/s $\Delta T_{exp} = 10$–30 K are correlated by the theoretical relation $Gr^*_{\delta_r} = 190(a'\delta_r)^{*3}$ to within an error of ±10%.

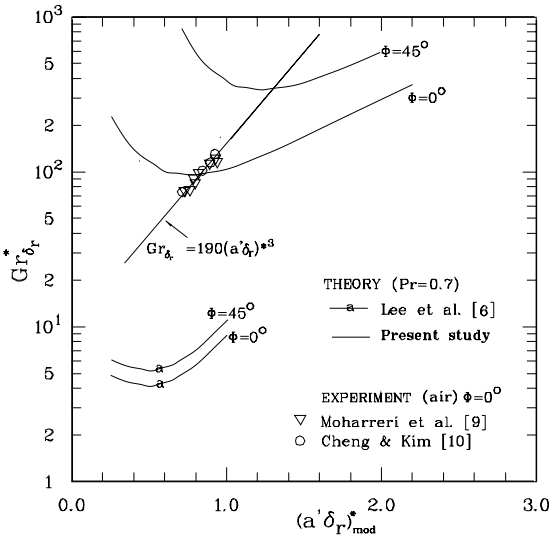

Fig. 5. The relation between the critical values $Gr^*_{\delta_r}$ and modified wave number $(a'\delta_r)_{mod}$.

Table 2
Onset position x^* for criterion $Nu_p/Nu_b = 0.1$[a]

ϕ (deg)	$Pr = 0.7$ ($a^* = 1.38$)			$Pr = 7.0$ ($a^* = 3.45$)		
	x^*	$Gr^*_{\delta_r}$	$a'^*\delta_r$	x^*	$Gr^*_{\delta_r}$	$a'^*\delta_r$
0	0.380	117	0.851	0.182	38.8	1.47
5	0.404	128	0.877	0.186	40.0	1.49
10	0.416	134	0.890	0.192	42.0	1.51
15	0.458	155	0.934	0.202	45.4	1.55
20	0.506	180	0.982	0.216	50.0	1.60
30	0.562	211	1.035	0.236	57.3	1.68
45	0.744	320	1.190	0.296	80.5	1.88
60	1.028	515	1.399	0.416	134	2.23
70	1.880	1289	1.892	0.756	329	3.00

[a] These values are evaluated by using $Gr_L/Re_L^{3/2} = 500$ and $t^0 = 10^{-4}$.

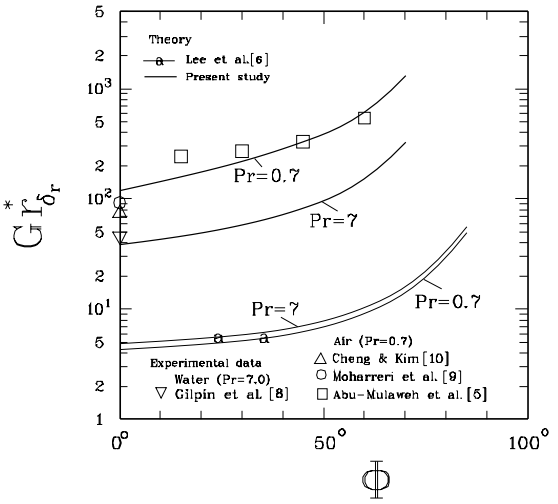

Fig. 6. Critical Grashof number $Gr^*_{\delta_r}$ vs. inclined angle ϕ.

The effect of inclined angle ϕ on the critical Grashof number $Gr^*_{\delta_r}$ is listed in Table 2 and shown in Fig. 6. It is observed from the data that an increase in the inclined angle ϕ increases the value of critical Grashof number $Gr^*_{\delta_r}$. The flow is more stable due to a decrease in buoyancy force in the normal direction. The critical Grashof number predicted by the previous study [6] was two orders of magnitude lower than the experimental data, However, the results of the present study show reasonable agreement with the previous experimental data [5,8–10]. It is also found that the Prandtl number has a destabilizing effect on the flow and the critical values of Grashof number decrease with an increase in the Prandtl number.

5. Conclusions

1. The effect of inclined angle from the horizontal on the stabilization of the thermal instability in mixed convection boundary layers is studied numerically by using heat transfer rate onset criterion and a linear instability model.
2. An increase in the inclined angle ϕ increases the value of critical Grashof number $Gr^*_{\delta_r}$. The flow is more stable due to a decrease in buoyancy force in the normal direction. The effects of inclined angle on the Nusselt number are less pronounced when the values of inclined angle ϕ increases.
3. The Prandtl number has a destabilizing effect on the flow and the critical values of Grashof number decrease with an increase in the Prandtl number. The results of the present study show reasonable agreement with the previous experimental data.

Acknowledgements

The authors would like to acknowledge the National Science Council of ROC for its financial support of the present work through project NSC 89-2212-E-233-009.

References

[1] W.M. Kays, A.L. London, Compact Heat Exchanger, third ed, McGraw-Hill, New York, 1984.
[2] F.P. Incropera, Convective heat transfer in electronic equipment cooling, ASME J. Heat Transfer 110 (1988) 1097–1111.
[3] G. Evan, R. Grief, A study of traveling wave instabilities in a horizontal channel flow with application to chemical vapor deposition, Int. J. Heat Mass Transfer 32 (5) (1989) 895–911.
[4] T.S. Chen, A. Moutsoglou, B.F. Armaly, Thermal instability of mixed convection flow over inclined surfaces, Numer. Heat Transfer 5 (1982) 343–352.
[5] H.I. Abu-Mulaweh, B.F. Armaly, T.S. Chen, Instabilities of mixed convection flows adjacent to inclined plates, ASME J. Heat Transfer 109 (1987) 1031–1033.
[6] H.R. Lee, T.S. Chen, B.F. Armaly, Nonparallel thermal instability of mixed convection flow on non-isothermal

horizontal and inclined flat plates, Int. J. Heat Mass Transfer 35 (8) (1992) 1913–1925.

[7] G.J. Hwang, M.H. Lin, Estimation of the onset of longitudinal vortices in a laminar boundary layer heated from below, ASME J. Heat Transfer 117 (1995) 835–842.

[8] R.R. Gilpin, H. Imura, K.C. Cheng, Experiments on the onset of longitudinal vortices in horizontal Blasius flow heated from below, ASME J. Heat Transfer 100 (1978) 71–77.

[9] S.S. Moharreri, B.F. Armaly, T.S. Chen, Measurements in the transition vortex flow regime of mixed convection above a horizontal heated plate, ASME J. Heat Transfer 110 (1988) 358–365.

[10] K.C. Cheng, Y.W. Kim, Vortex instability phenomena relating to the cooling of a horizontal isothermal flat-plate by natural and forced laminar convection flows, in: W. Aung (Ed.), Cooling Technology for Electronic Equipment, Hemisphere, Washington DC, 1988, pp. 169–182.

[11] S.L. Lee, Weighting function scheme and its application on multidimensional conservation equations, Int. J. Heat Mass Transfer 32 (11) (1989) 2065–2073.

[12] F.P. Incropera, A. Knox, J.R. Maughen, Mixed convection flow and heat transfer in the entry region of a horizontal rectangular duct, ASME J. Heat Transfer 109 (1987) 434–439.

[13] J.R. Maughen, F.P. Incorpera, Experiments on mixed convection heat transfer for airflow in a horizontal and inclined channels, Int. J. Heat Mass Transfer 30 (7) (1987) 1307–1318.

[14] F.C. Chou, C.S. Han, Wall conduction effect on the onset of thermal instability in horizontal rectangular channel, Exp. Heat Transfer 4 (1991) 355–365.

[15] T. Fujii, H. Imura, Natural convection heat transfer from a plate with arbitrary inclination, Int. J. Heat Mass Transfer 15 (4) (1972) 755–767.

[16] K.C. Cheng, T. Obata, R.R. Gilpin, Buoyancy effects on forced convection heat transfer in the transition regime of a horizontal boundary layer heated from below, ASME J. Heat Transfer 110 (1988) 596–603.